Experimental and numerical studies of reinforced concrete stair beams strengthened with steel bars and plates

Engineering Structures 297 (2023) 117037

Contents lists available at ScienceDirect

Engineering Structures

journal homepage: www.elsevier.com/locate/engstruct

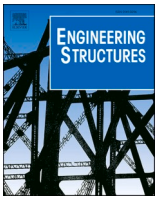

Experimental and numerical studies of reinforced concrete stair beams strengthened with steel bars and plates

Ahmed Hamoda [a], Mahmoud A. El-Mandouh [b], Mizan Ahmed [c], Aref A. Abadel [d], Qing Quan Liang [e,*], Galal Elsamak [a,f]

[a] Department of Civil Engineering, Faculty of Engineering, Kafrelsheikh University, Kafrelsheikh, Egypt
[b] Department of Civil Engineering, Faculty of Engineering, Beni-Suef University, Egypt
[c] Centre for Infrastructure Monitoring and Protection, School of Civil and Mechanical Engineering, Curtin University, Kent Street, Bentley, WA 6102, Australia
[d] Department of Civil Engineering, College of Engineering, King Saud University, Riyadh 11421, Saudi Arabia
[e] College of Sport, Health, and Engineering, Victoria University, PO Box 14428, Melbourne, VIC 8001, Australia
[f] Department of Civil Engineering, Delta Higher Institute for Engineering & Technology, Talkha, Egypt

ARTICLE INFO

Keywords:
Stair beams
Strengthening
Steel sheets
Stainless steel strips
Finite element modeling

ABSTRACT

The bends under sagging moments in a Reinforced Concrete Stair Beam (RCSB) in staircases may be damaged because of improper detailing design or construction; therefore, they need to be strengthened or repaired. The structural behavior of strengthened RCSBs has not been investigated adequately. This paper presents experimental and numerical investigations on the flexural strengthening of RCSBs with bends under sagging moments. Tests on RCSBs were undertaken that were strengthened by using either the Near-Surface Mounted Steel Bars (NSMSBs) or the Externally Bonded Steel Plates (EBSPs). Three steel materials were employed, including Steel Bars (SBs), Steel Sheets (SSs) and Stainless-Steel Plates (SSPs). The test program and outcomes are described in detail of six full-scale strengthened RCSBs loaded up to collapse. A finite element model is developed employing ABAQUS to simulate the performance of the tested RCSBs. It is found that the utilized strengthening techniques effectively enhance both the cracking and ultimate loads in addition to the energy absorption capacity. The agreement between simulations and experiment is good, suggesting that the model of nonlinear finite element analysis can be used with confidence to perform further parametric instigations.

1. Introduction

Reinforced Concrete Stair Beams (RCSBs) are often used to support the stair slabs in multi-story Reinforced Concrete (RC) buildings. The bends in a RCSB under sagging moments may be damaged. As reported by Li and Mosalam [1], the 8.0 Mw earthquake in Sichuan, China led to severe damage to the existing buildings or the collapse of structures. Field studies afterwards the earthquake found that in some cases, stair beams were damaged more severely than the main structures. Bechtoula and Ousalem [2] reported the similar outcome from the field studies afterward 2003 Algeria earthquake. Wrong detailing of opening bends/joints could also result in the spalling of concrete cover and the development of cracks at the opening bend, as illustrated in Fig. 1 [3]. The need to strengthen existing stair beams has often been overlooked compared to main structures. Strengthening of structures or a portion of a structure is often required to meet the demand for additional load-bearing capacity. Similarly, strengthening of opening bends in the stair beams may be required for retrofitting purposes. However, strengthening the opening bend in the stair beams has been rarely investigated.

There are various techniques used to strengthen structures such as concrete patching, adding an additional layer of cementitious material, enlarging cross-section, bonding external steel plates, and bonding carbon fiber. Fiber Reinforced Polymer (FRP) materials have been widely used in strengthening structures due to their high tensile strength and corrosion resistance. Modified fiber-reinforced concrete materials, such as engineered cementitious concrete (ECC), have been developed that exhibit high strain-hardening performance and have high strain capacity in tension besides having high compressive and tensile strength [4–10]. Researchers investigated the effectiveness of ECC in retrofitting structural elements subjected to various loading conditions [9,11–14]. Hamoda et al. [15] studied the effects of ECC on the torsional behavior

* Corresponding author.
E-mail address: Qing.Liang@vu.edu.au (Q.Q. Liang).

https://doi.org/10.1016/j.engstruct.2023.117037
Received 20 May 2023; Received in revised form 4 October 2023; Accepted 8 October 2023
Available online 13 October 2023

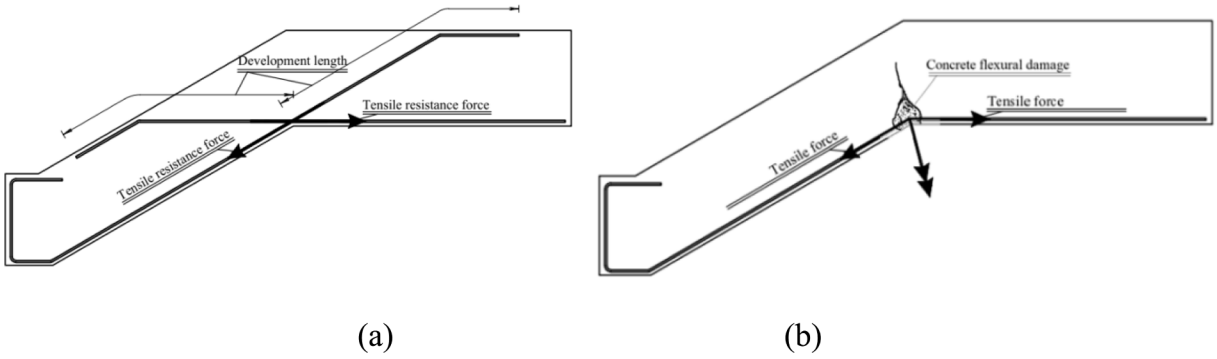

Fig. 1. Reinforcement details in the opening bend of RCSB: (a) Right details and (b) Wrong details.

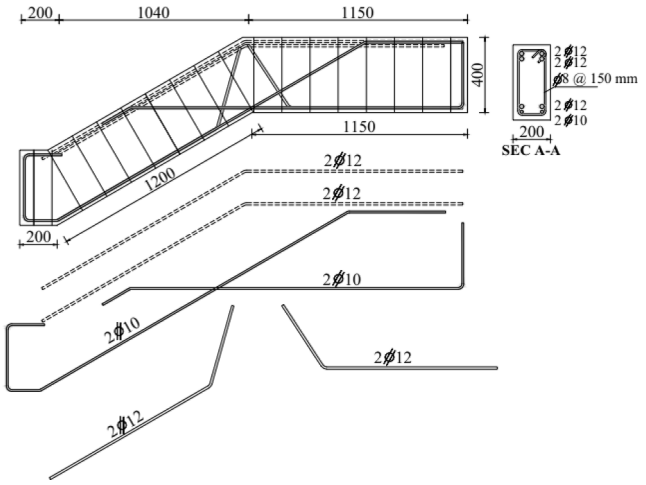

Fig. 2. Dimension and reinforcement details of the reference beam (B0).

of steel–concrete composite joints. It was found that the structural performance of composite joints with ECC is much higher than that of composite joints made of Normal Concrete (NC) in terms of strength and energy absorption. Emara et al. [16] carried out tests on ECC columns loaded concentrically. Test results showed that ECC columns exhibited thin cracks and improved load-carrying capacity.

Stainless steel is often used in the construction industry due to its strain-hardening characteristics and excellent corrosion resistance. Recently, researchers have studied the applicability of Stainless Steel Plates (SSPs) in the strengthening of structural elements. Hamoda et al. [7,9] studied the performance of RC beams strengthened with ECC and SSPs subjected to various loading. It was reported that the flexural and shear strengths of a RC beam can be improved significantly using ECC and SSPs.

Externally Bonded Steel Plates (EBSPs) with adhesive materials have been used to strengthen reinforced concrete members [17]. The most widely used adhesive material is epoxy. These adhesive materials need good preparation of the concrete surface to remove the external weak layer that may cause poor and inappropriate attachment [18]. Rasheed et al. [19] found out that the EBSP strengthening system results in higher tensile capacity of RC members and better durability to rain and cold weather than the technique using Near Surface Mounted Steel Bars (NSMSBs). However, these advantages can be realized only if the strengthening is properly treated [20–25].

The closely spaced rebars in star beams may hinder the flowability and passing ability of concrete in narrow gaps. The microstructures of concrete e.g. flowability and high-passing ability of concrete are important to ensure that the concrete pass-through narrow gaps of reinforcement and reach the corners of formwork [26–28]. The flowability and passing ability of concrete in composite columns can be improved by using cementitious fillers and inert filler proposed by Lai et al. [29]. The cementitious fillers such as ground granulated blast furnace slag can also improve the heat resistance and residual strength of concrete [30]. In addition, increasing wet packing density can improve the passing ability of concrete in narrow places [31]. Lai et al. [32] used cementitious fillers, such as silica fume and fly ash to improve the wet packing density of concrete in order to increasing the flowability of heavy-weight concrete.

This study investigates the flexural performance of RCSBs where the opening bends are strengthened by using either EBSPs or NSMSBs. Tests were carried out on six full-scale RCSBs subjected to flexural loads. Different strengthening techniques and configurations have been implemented including: (a) bonding two bottom bars facing each other at the opening joint with different development lengths inside the RCSBs to study the effectiveness of the NSMSBs technique; (b) bonding a steel sheet with anchorage bolts at the bottom surface of the opening joint using the EBSPs technique; (c) bonding SSPs at the RCSBs bottom surface with two surrounding SSPs around the RC beam applying EBSPs technique; (d) and bonding SSPs at both sides of the RC beam representing EBSPs technique. The experimental program and results obtained are presented. A finite element model is developed to simulate the test behavior of such beams and verified by test data.

2. Test program

2.1. Specimens

The experimental program was designed to test six-full scale RCSBs including one control beam (B0) without strengthening and five RC beams (B1-B5) with various strengthening techniques. The dimensions and details of the main reinforcement of each were identical. The angel of the tested stair beams was very close to the angel of the real-life RC stair beams. Each stair beam had a span of 2550 mm, a width of 200 mm, and a thickness of 400 mm. It was divided into three parts: two horizontal parts with lengths of 1150 mm and 200 mm, respectively, and the last inclined part with a length of 1200 mm with an angle of 1 (vertical): 2 (horizontal), which corresponded to the slope of a typical flight of RC stairs as illustrated in Fig. 2. In the preliminary design of the specimens, a finite element analysis on the stair beam was initially performed to ensure the specimens failed in bending mode rather than shear failure. Shear failure often occurs in a beam where the load is applied close to the support or for a span with a short overhang. To avoid shear failure, the length of the horizontal and inclined parts of the specimens was almost the same and the applied load was approximately at the center of the horizontal and inclined parts of the specimens. Design consideration of the shear is beyond the scope of this study. All tested beams had 2 rows of bars with 10 and 12 mm diameter in flexure. In order to avoid local compression failure during the test, 0.48 % flexural reinforcement ratio was considered which was below the maximum ratio permitted by

Fig. 3. Wooden formworks and field casting process.

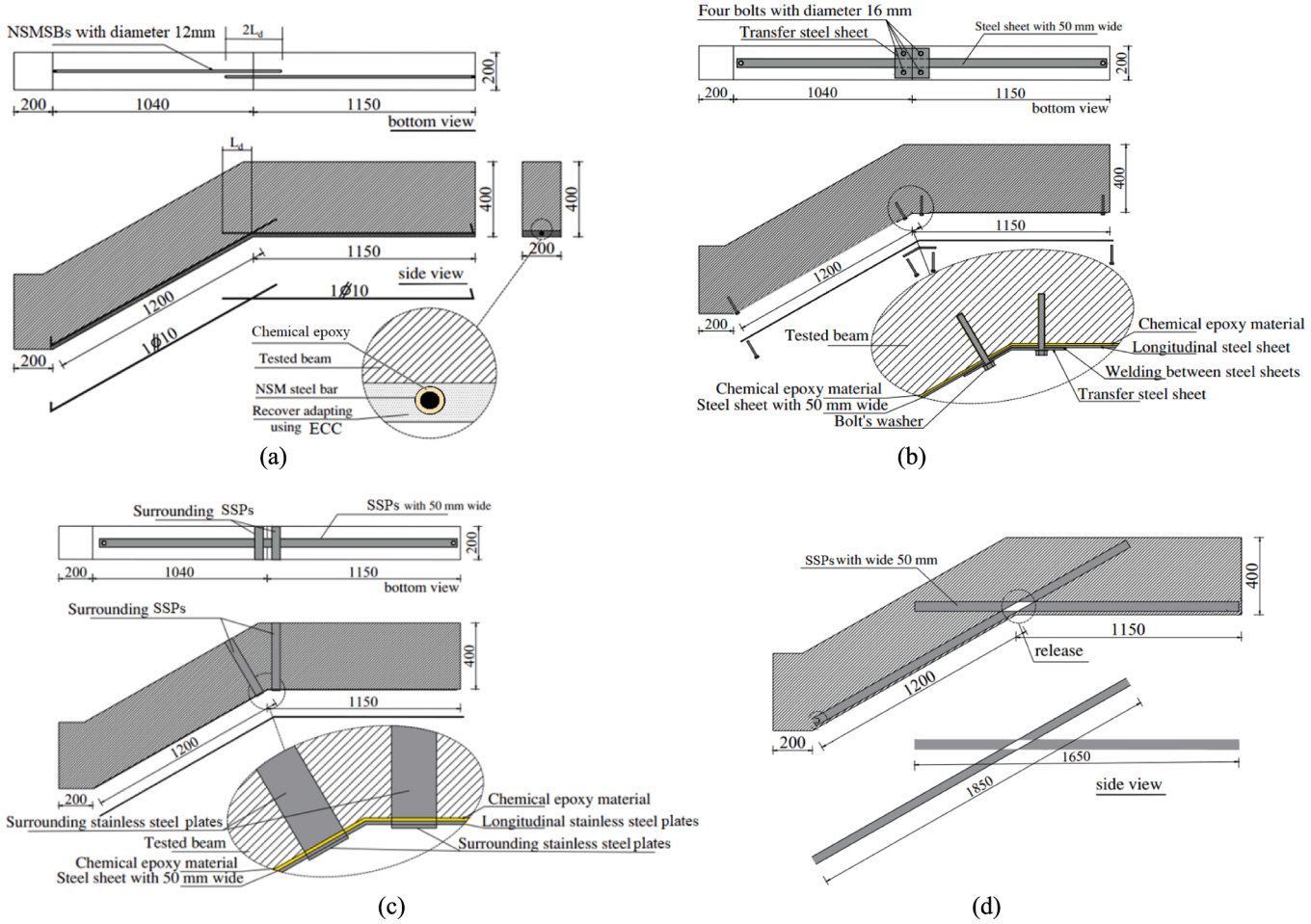

Fig. 4. Geometric details of strengthened beams: (a) Beams B1 and B2, (b) Beam B3, (c) Beam B4, (d) Beam B5.

the ACI 318–19 [33]. In this context, the strengthening reinforcement ratios were selected with consideration of suppressing the probable unwanted compression or shear collapse. The compression reinforcement of all beams consisted of four bars of 12 mm diameter to prevent compression failure as illustrated in Fig. 2. All beams were reinforced with stirrups of 8-mm diameter with a spacing of 150 mm. The thickness of the SPs and the diameter of the bars were selected based on the availability of the materials in the local markets and the preliminary results obtained from FE models to ensure the ultimate load was within the maximum capacity of the testing machine. In order to ensure the total tensile forces provided by the steel bars, SSP, and SS on the stair beams were similar for the comparison purposes, materials with a very similar yield strength available on the market were chosen for this study. The yield strengths of the 10-mm steel bars, 12-mm steel bars, SSP, and SS were measured as 384, 415, 466, and 406 MPa, respectively. However, it should be mentioned that regardless of the similar yield strength of conventional steel bars and stainless-steel materials, due to the distinguished strain hardening performance, SSP, and SS provide higher tensile force under loading. Therefore, it is not rational to expect that the performance of stair beams reinforced with different materials is the same.

All beams were cast with NC at the same time with the same compressive strength as can be seen in Fig. 3. Beam B1 was strengthened by bonding two bars at the tension side with a diameter of 12 mm facing each other at the opening joint with a development length (L_d) equal to twenty times the bar diameter ($20D_b$) as shown in Fig. 4a. The method of

(a)

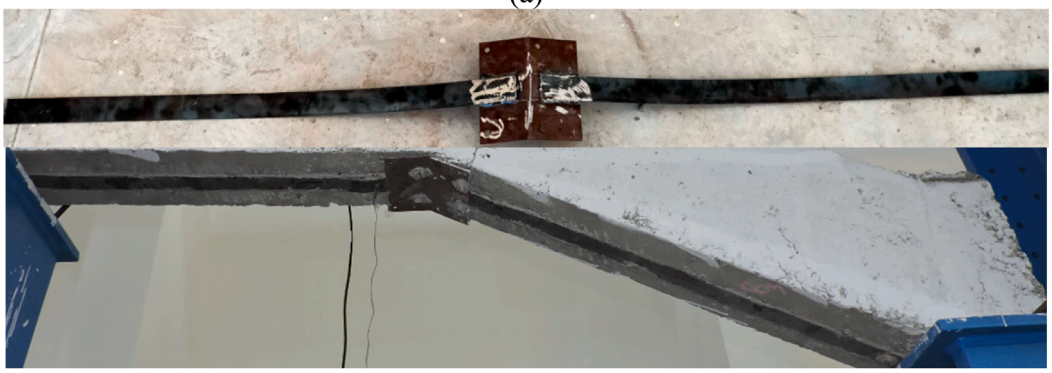

(b)

(c)

(d)

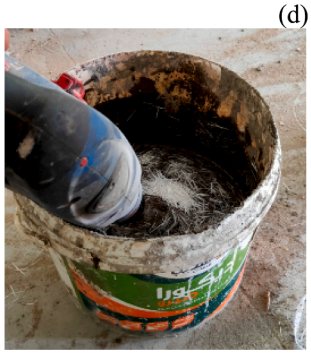

(e)

Fig. 5. Strengthening preparation and adapting: (a) embedded steel bars in B1 and B2; (b) bonding of and adapting of steel sheets for B3; (c) bonding of SSPs used for B4; (d) bonding of SSPs used for B5; (e) ECC mechanical mixing used as concrete re-covering for B1.

Table 1
Test matrix and method of strengthening.

Specimen's ID	Concrete type	Strengthening technique	L_d	Thickness of SPs (or) bar diameter	Figure
B0	NC	————		————	Fig. 2
B1	NC + ECC	NSMSBs	$20D_b$	$D_b = 12$ mm	Fig. 4
B2	Recover		$25D_b$		(a)
B3	NC	EBSPs with SSs	——	$t_s = 1$ mm	Fig. 4 (b)
B4	NC	* EBSPs with SSPs	——	$t_s = 1$ mm	Fig. 4 (c)
B5	NC	** EBSPs with SSPs	——	$t_s = 1$ mm	Fig. 4 (d)

Note:- NSMSBs: Near-Surface Mounted Steel Bars; EBSPs: Externally Bonded Steel Plates; SBs: Steel Bars SSs: Steel Sheets; SSPs: Stainless Steel Plates.
* Lower SSP with two surrounding SSPs around the beam at the opened-joint shown Fig. 4(c).
** SSPs at both sides of RC beams shown Fig. 4(d).

strengthening for specimen B2 was similar to specimen B1 but the development length was equal to $25D_b$. It should be notes that the development lengths were selected with respect to previous recommendations [34–36]. Beam B3 was strengthened by bonding Steel Sheets (SSs) at the tension side along the bottom surface with anchorage bolts at the opening joint and having a width of 50 mm and thickness of 1 mm as shown in Fig. 4b. The strengthening of beam B4 was similar to that of beam B3 but SSP was used and the anchorage bolts were replaced by two surrounding SSPs around the beam at the opening joint as illustrated in Fig. 4c. The beam B5 was strengthened from the two sides by bonding SSPs with a width and thickness of 50 mm and 1 mm, respectively, as illustrated in Fig. 4d. It should be noted that the beams had to be lifted and hung up using a crane in order to replicate the real-life strengthening from underneath the beam. Therefore, the safety of the person involved in the strengthening could not be guaranteed due to the scale and weight of the test specimens. Due to safety concerns, the beams were therefore flipped upside down as illustrated in Fig. 5 to perform the strengthening. However, in real-life, the stairs are connected to the main structures and sufficient room is available to do the strengthening from underneath without any issues. Therefore, the quality of the strengthening should not be a concern. Table 1 presents the details of the method of strengthening of the RC stair beams. The strengthening techniques and preparations can be detailed in the following sections.

2.2. Strengthening with bottom steel reinforcement

When adding an additional layer of concrete to the RC beam, care should be given due to the difference in the motions between the additional layer and RC element caused by shrinkage, temperature variations or both. These would cause durability problems [37,38]. As a result, there may be some cracking and delamination along the zone where the two materials meet. Hence, it is crucial to use appropriate connectors to bond the two layers and/or to properly prepare the surface [39,40].

The beams B1 and B2 were strengthened with two bottom reinforcing bars face to face at the opening joint with a diameter of 12 mm and L_d inside the concrete equal to twenty and twenty-five bar diameters, respectively, as shown in Table 1. The schematic design and details of strengthening can be seen in Fig. 4a. The construction process of the beams B1 and B2 was as follows; (a) formwork was prepared and reinforcements were placed as illustrated in Fig. 3; (b) the cast was implemented in the field as shown in Fig. 3; (c) the formwork was removed after few days then the RC beams were left to cure for 28 days; (d) the bottom concrete cover was removed until the tensile beam

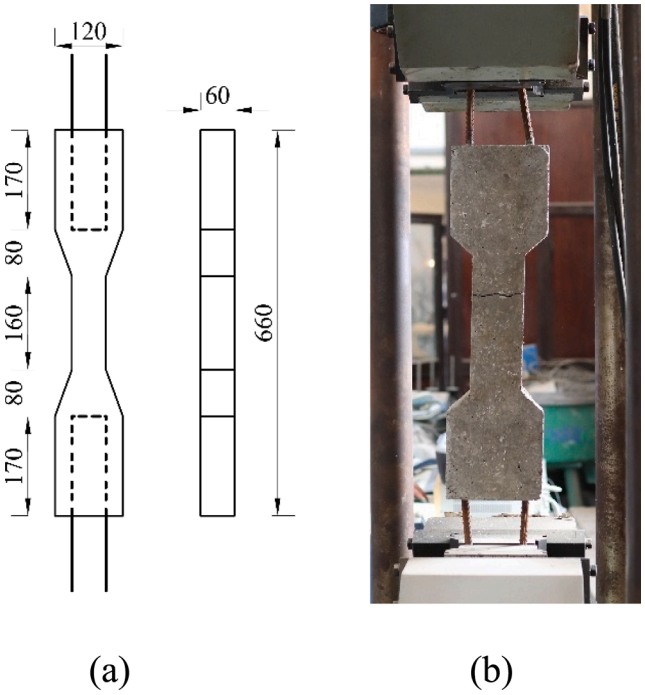

Fig. 6. Uniaxial tensile tests observed experimentally: (a) concrete dimensions; (b) test set-up and failure model of NC.

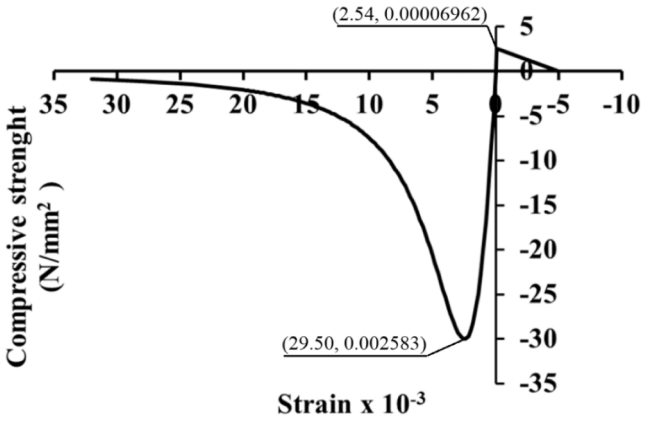

Fig. 7. Uniaxial stress–strain law for NC.

Table 2
Mix proportion and concrete compressive strength.

Concrete	Cement (kg/m^3)	Fine aggregate (kg/m^3)	Coarse aggregate (kg/m^3)	Fly ash (kg/m^3)	Water/binder	polypropylene Fiber (%) in volume	HRWR (kg/m^3)	f_c' (MPa)	Poisson Ratio
NC	350	700	1150	—	0.43	—	—	29.5	0.2
ECC	552	442	—	602	0.25	2.00	14.42	44.19	0.22

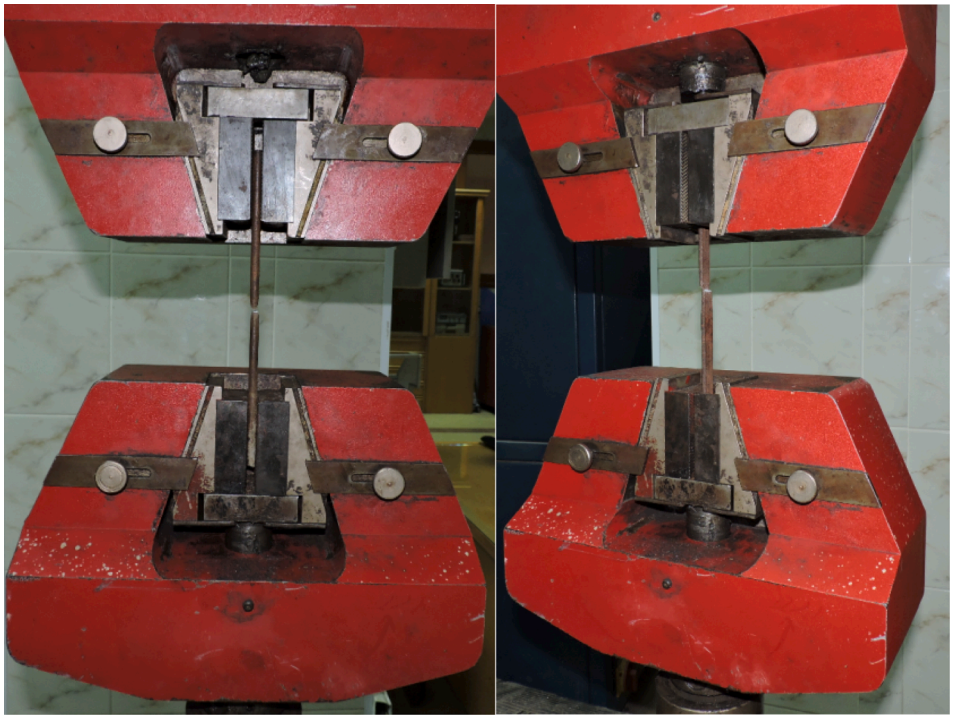

Fig. 8. Uniaxial tensile tests observed experimentally for steel elements.

Table 3
Material properties of steel elements.

Steel element	Yield strength		Ultimate tensile strength		Modulus of elasticity, E (GPa)	Poisson Ratio
	σ_y (MPa)	ε_y(%)	σ_u (MPa)	ε_u(%)		
8 mm bar	296	0.16	565	12.9	189	0.30
10 mm bar	384	0.20	640	12.2	194	0.30
12 mm bar	415	0.21	691	11.3	194	0.30
SSP	466	0.22	745	11.4	205	0.29
SS	406	0.21	610	10.5	198	0.28

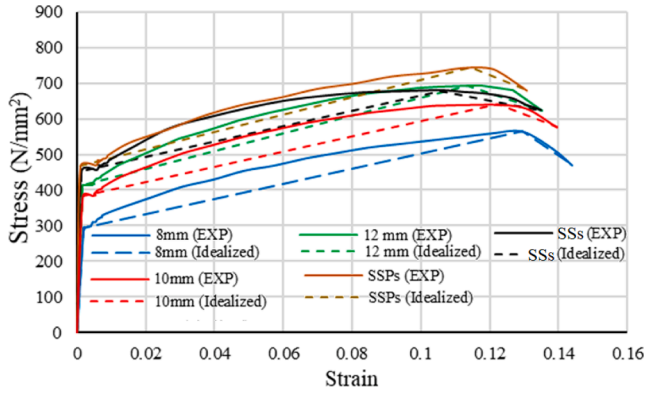

Fig. 9. Measured and idealized stress–strain curves of steel elements.

reinforcement bars were exposed; (e) planting reinforcing bar anchoring adhesive regime was used herein as follows: two holes (with lengths of 240 mm and 300 mm achieving 20 and 25 times of bar diameter for beams B1 and B2, respectively) and a diameter of 12 mm were made inside the concrete at the extension surface of the straight and inclined parts of the lower surface of the RC beams by using a drilling machine to achieve the development length (f) using air pressure, the specimen's bottom surface and two holes were cleaned to remove dust (g) epoxy was used at the bottom surface of the RC beam and all holes were filled (h) two steel bars with a diameter of 16 mm were glued at the centerline of the bottom surface of the RC beam one at the bottom straight part of the beam and the other at the inclined surface part of the beam facing each other at the opened-joint and the two ends of the steel bars were placed in the holes at the opened-joint as illustrated in Fig. 5a and (i) ECC was mechanically mixed as shown in Fig. 5e with proportions presented in Table 2 in order to cover the bottom concrete surface.

2.3. Strengthening with bottom steel sheets

Beam B3 was strengthened with SSs with a width of 50 mm and 2100 mm of total length welded together with a square steel plate (200 × 250 mm) as illustrated schematically in Fig. 4b. The tensile stresses developed in the opening joint in the RC beam under vertical load can be resisted by steel sheets and anchorage bolts. The beam B3 was constructed as follows: (a) after curing the beam for 28 days, the bottom surface of the B3 was cleaned well; (b) two holes having the diameter of 16 mm at the steel sheets were made as well as in the RC beam with a depth of 90 mm using a drilling machine; (c) by using air pressure, the specimen's bottom surface, and all holes were cleaned well; (d) epoxy was used at the bottom surface and all holes were filled; and (e) the steel sheets were attached to the tensile surface and anchored with bolts. The embedded length of the anchored bolts was 90 mm. The experimental preparation of beam B3 is illustrated in Fig. 5b.

2.4. Strengthening with bottom and side SSPs

The strengthening process of beam B4 was similar to that of beam B3 with a difference in the steel sheet as shown schematically in Fig. 4c. The steel sheet of beam B4 was continuous and made of SSPs with a length of 2330 mm and was attached to the tension surface of the RC beam using chemical epoxy as illustrated in Fig. 5c. Two surrounding SSPs were bonded to the RC beams using epoxy at the opened joints to resist tensile

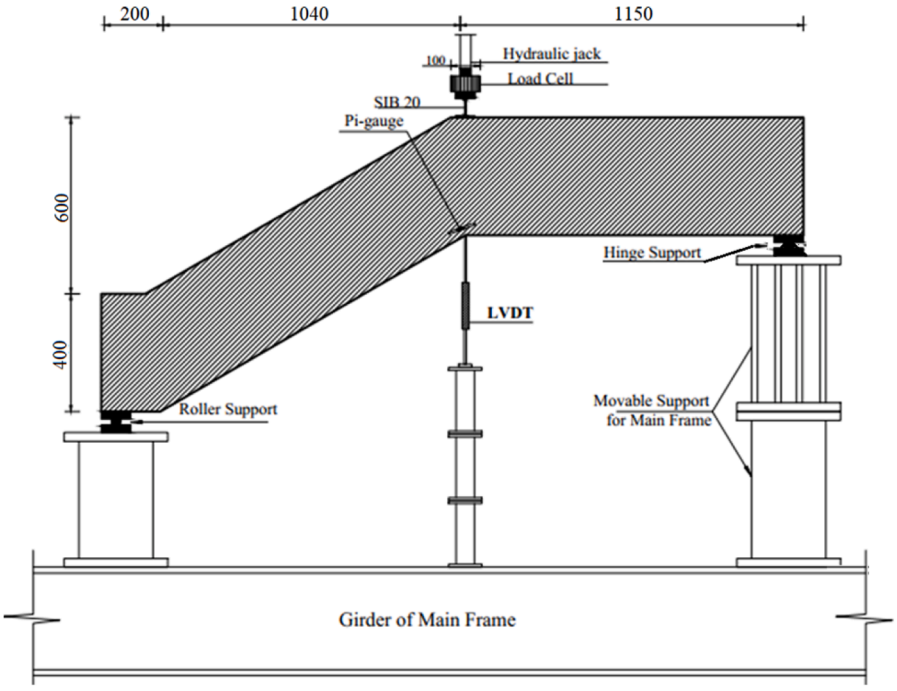

(a)

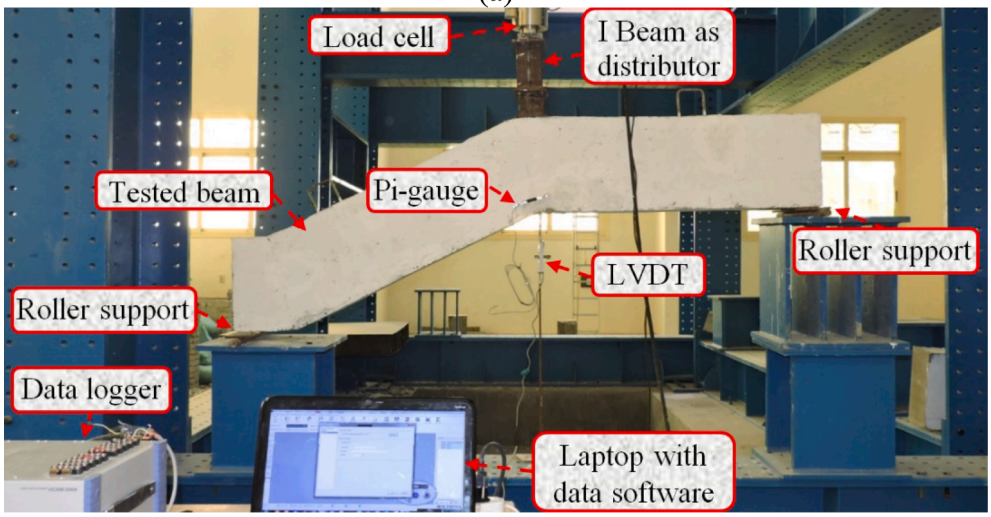

(b)

Fig. 10. Test set-up and instrumentation: (a) schematic illustration; (b) actual set-up.

Table 4
Experimental results.

Specimen ID	Cracking Stage				Yield Stage			Ultimate Stage		Max deflection	Ductility index	Absorbed Energy	Failure Mode*
	P_{cr} (kN)	P_{crB}/P_{crB0}	Δ_{cr} (mm)	W_{cr} (mm)	P_y (kN)	P_{yB}/P_{yB0}	Δ_y (mm)	P_u (kN)	P_{uB}/P_{uB0}	Δ_u (mm)	(DI) Δ_u/Δ_y	(E) (kN.mm)	
B0	66	1.00	3.89	0.23	97	1.00	8.02	110	1.00	28.41	3.54	2497	**F**
B1	106	1.61	4.01	0.19	143	1.47	7.22	162	1.47	44.38	6.15	6430	**F + B_p**
B2	116	1.76	3.56	0.16	151	1.56	6.05	170	1.55	52.57	8.69	7496	**F + B_p**
B3	83	1.26	3.54	0.21	110	1.13	5.61	120	1.09	19.87	3.54	1105	**F + SS_d**
B4	91	1.38	3.61	0.21	110	1.13	5.36	136	1.24	45.32	8.46	5539	**F + SSP_d**
B5	101	1.53	4.02	0.19	118	1.22	4.91	137	1.25	35.89	7.31	4390	**F + SSP_d**

Note:- P_{cr} = cracking load, P_y = yield load, P_u = ultimate load; Δ_{cr} = deflection recorded at P_{cr}, $\Delta_{y=}$ deflection recorded at P_y, Δ_u = maximum deflection, and W_{cr} = cracking width measured at P_{cr}, ***F:** Flexural failure; **B_p:** Pulling-out of embedded bars; **SS_d:** de-bonding of steel sheet; and **SSP_d:** de-bonding of SSP.

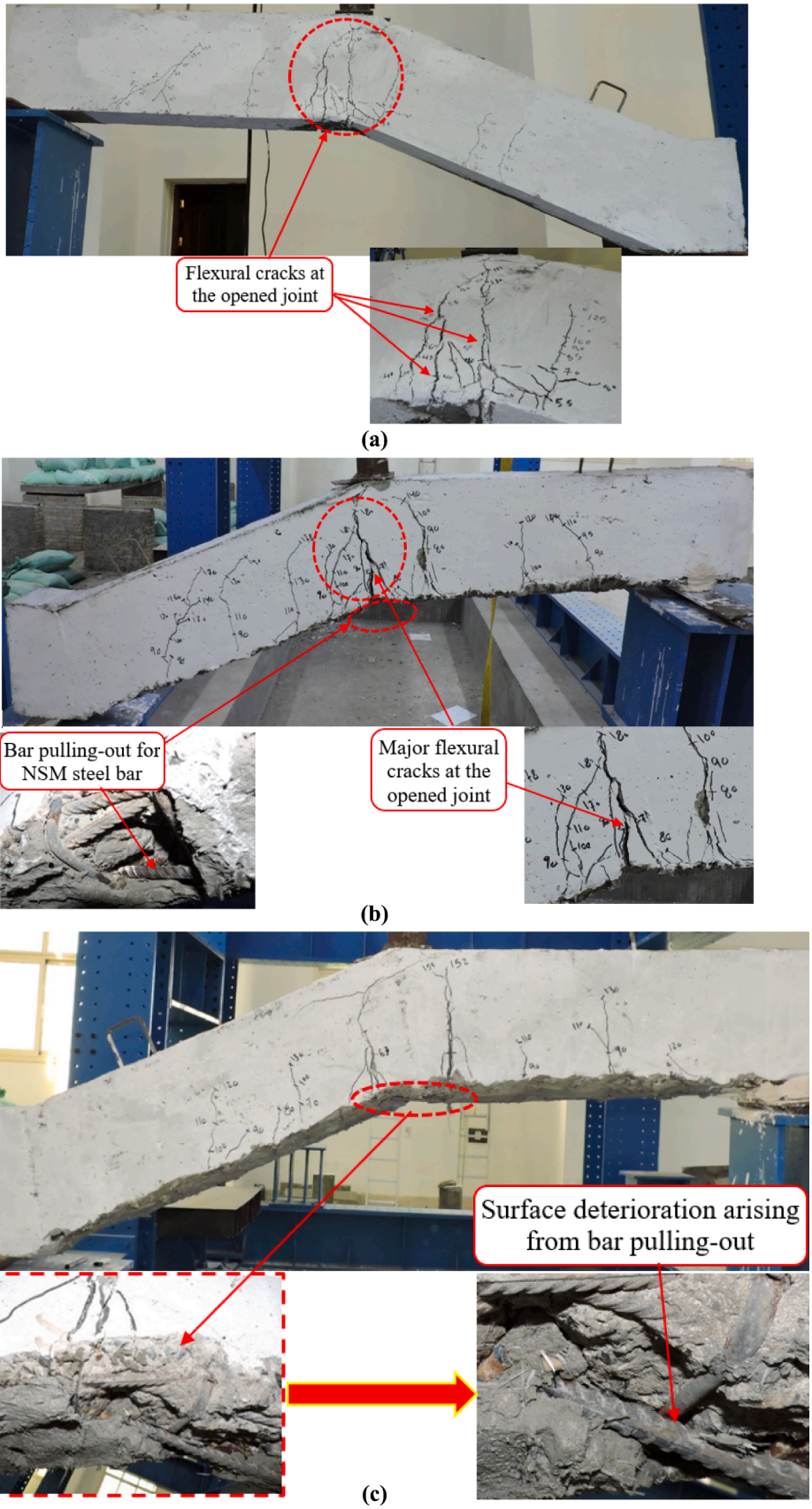

Fig. 11. Crack pattern and failure mode of tested beams: (a) master beam B0; (b) B1; (c) B2 (d) B3; (e) B4; (f) B5.

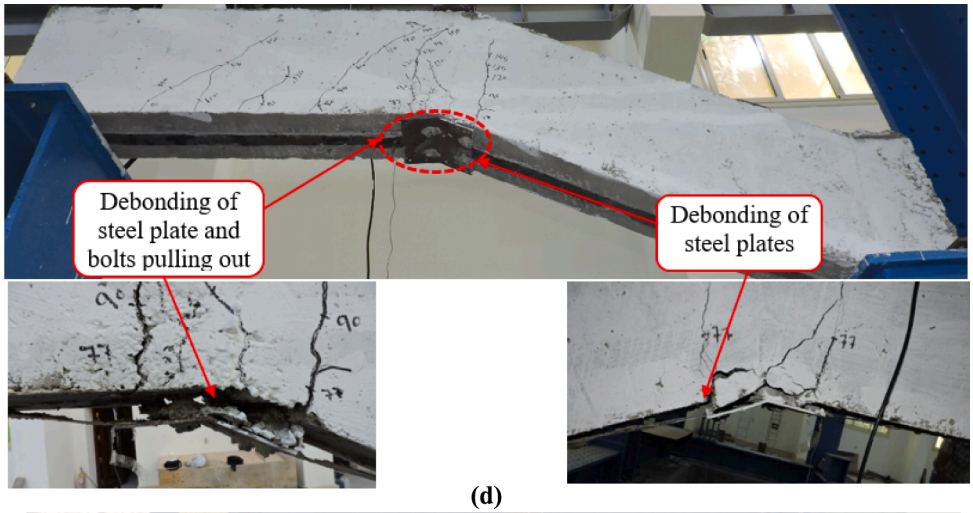

(d)

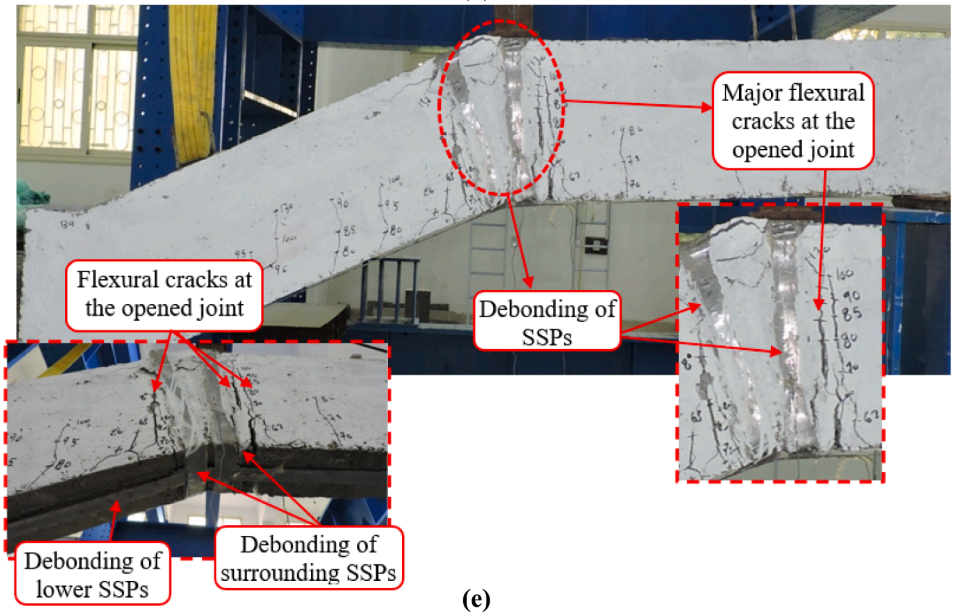

(e)

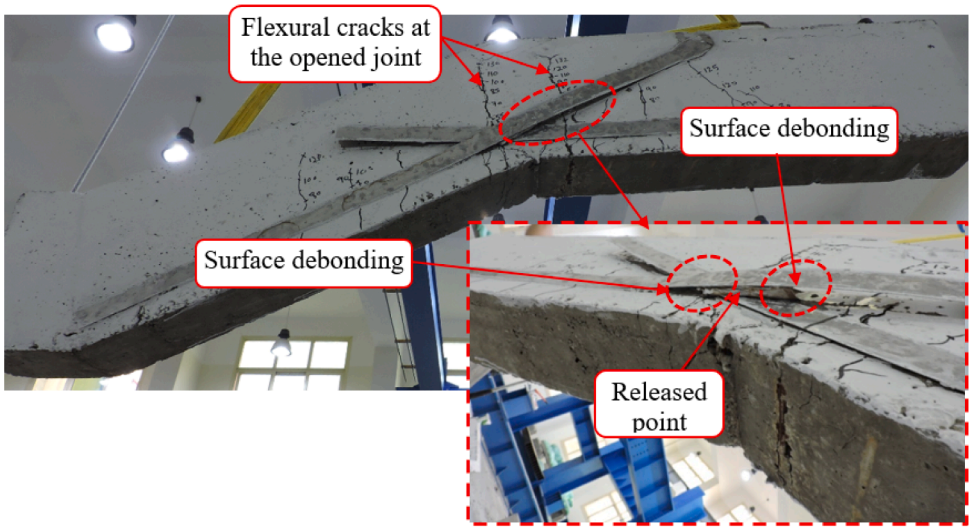

(f)

Fig. 11. (*continued*).

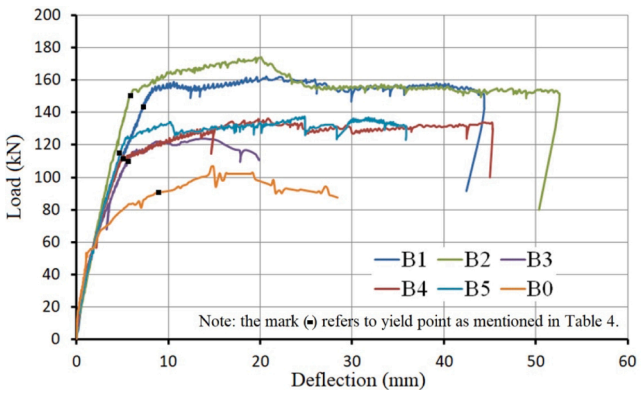

Fig. 12. Load-Deflection responses of the specimens.

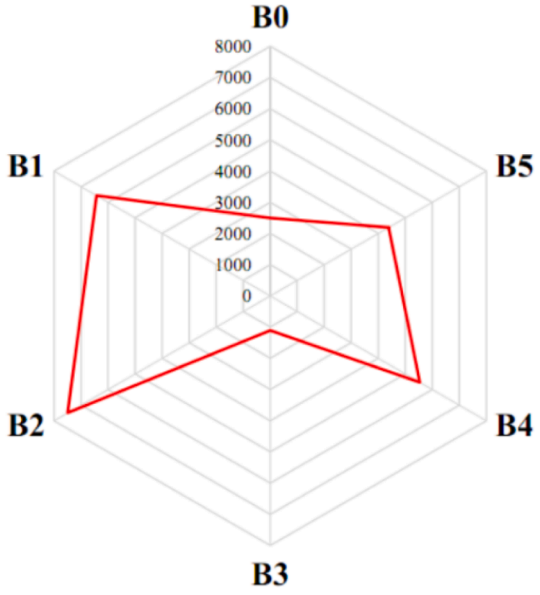

Fig. 13. The absorbed energy (*E*) values for all beams (kN.mm).

stress. The tensile resultant forces developed at the stair joint were carried by the two surrounding SSPs. The preliminary results obtained from FE models showed that the longer the length of the surrounding SSPs, the higher the bearing capacity of the beams. Therefore, the full depth of the beam (400 mm) was chosen as the length of the surrounding SSPs to prevent premature failure and to provide the maximum resistance to the tensile stresses.

Beam B5 was strengthened with two side SSPs as shown schematically in Fig. 4d. The purpose of this external strengthening was to simulate the internal reinforcing bars at the bottom of the beam. The specimen B5 was constructed by the following process: (a) after curing the beam for 28 days, the two sides of the RC beam were roughened; (b) the position of SSPs at all sides of the beam was perfectly cleaned; and (c) the SSPs were bonded with chemical epoxy as illustrated in Fig. 5d.

3. Material properties

Two types of concrete, namely NC and ECC were used to cast the tested beams. The ECC was only used in beams B1 and B2 at the bottom surface as a concrete cover layer. Table 2 presents the mix designs of both NC and ECC. The compressive concrete strength was determined by averaging the test results of three cylinders with a diameter of 150 mm and a length of 300 mm, cast at the same time as the tested beams. The concrete compressive strengths of the NC and ECC were about 29.90 N/mm^2 and 44 N/mm^2 as shown in Table 2. The tensile strength of different concrete was measured in the lab as shown in Fig. 6. The measured uniaxial tensile stress–strain curve for NC with about 2.54 N/mm^2 tensile strength is given in Fig. 7.

The steel bars with diameters of 10 and 12 mm were used as longitudinal reinforcements whereas the diameter of the stirrups was 8 mm. The material properties of each steel element were measured using tensile tests and the test set-up is shown in Fig. 8. The material properties of steel sheets and SSPs were measured from the tensile coupon test. The measured yield strength, ultimate tensile strength, elastic modulus and Poisson's ratio of steel elements are presented in Table 3. The recorded stress–strain curves for steel elements are shown in Fig. 9. The tensile strength of the anchorage bolts was 600 MPa according to the manufacturer.

4. Test setup

Fig. 10 shows the typical test setup of the tested beams. It should be noted that the beams were tested after 40 days and 35 days of casting NC

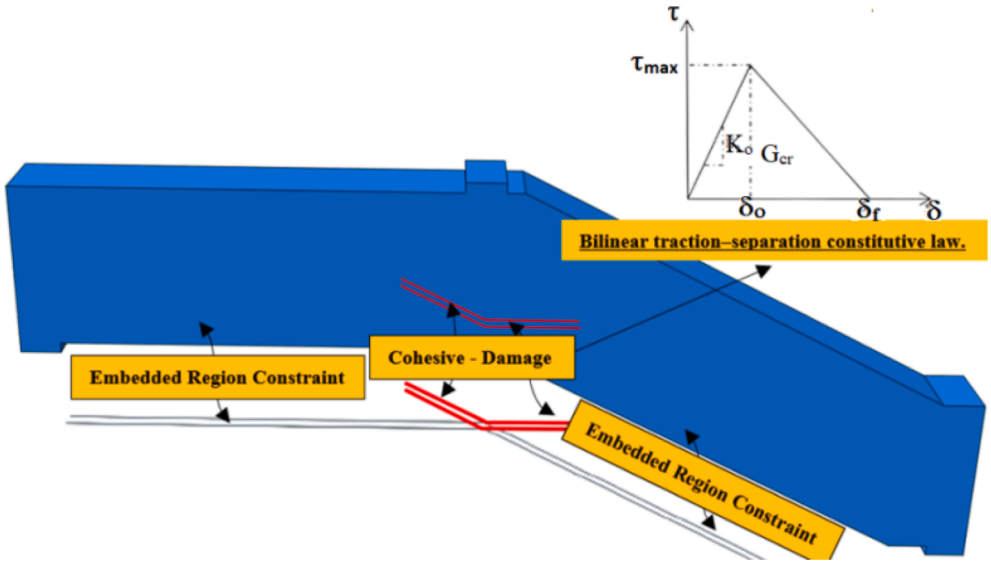

Fig. 14. Interaction between concrete-NSMSBs.

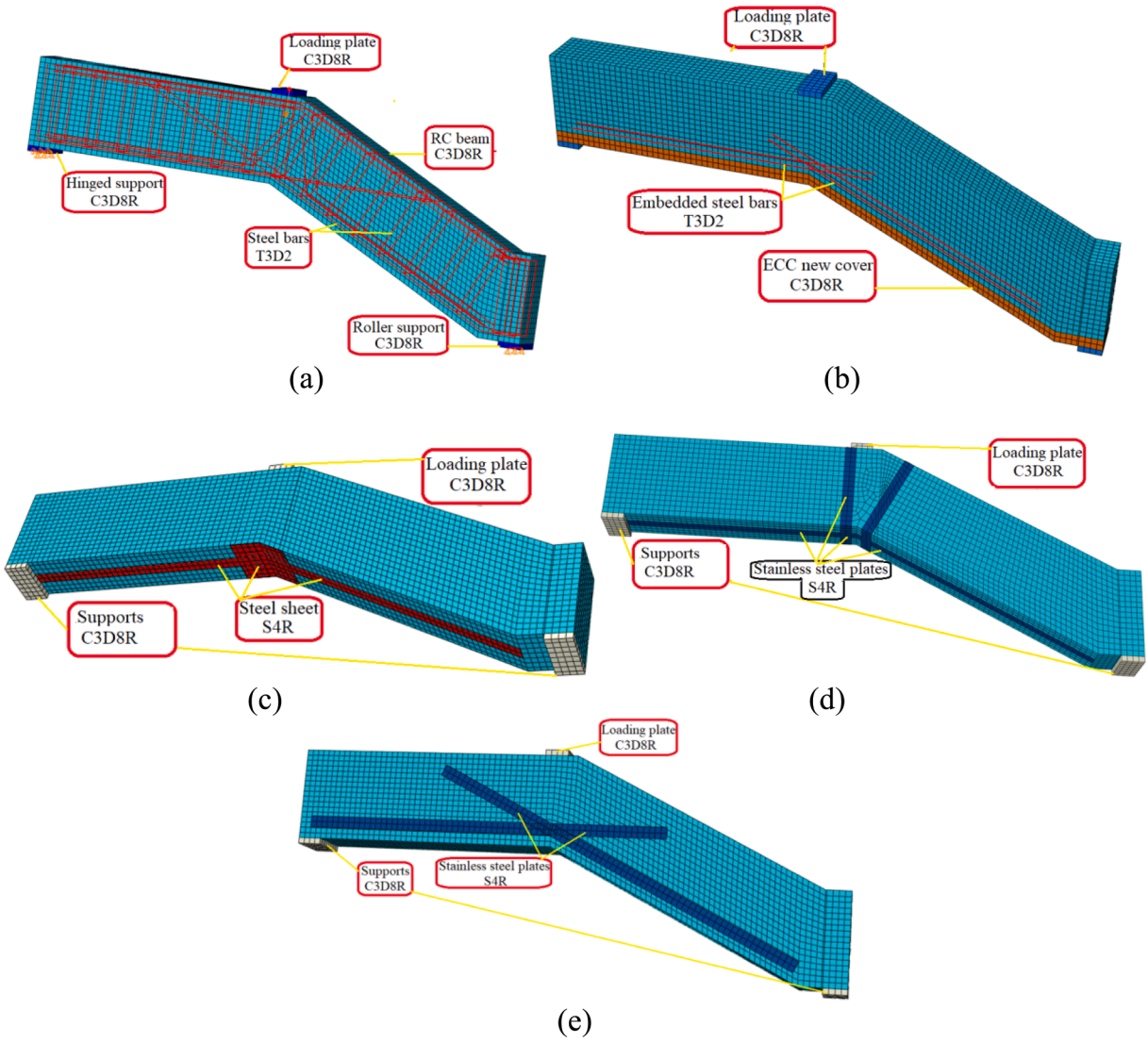

Fig. 15. Development of the FE: (a) B0; (b) B1andB2; (c) B3; (d) B4; (e) B5.

and ECC, respectively. Before the test, the tested beams were cleaned to remove dust and painted white for better visualization and to mark the cracks on the beams during the test. Considering the heavy weight of the beam, a steel crane was used to lift the beam and placed it on the loading machine as illustrated in Fig. 10. This study examined the performance of stair beams where the opening bend was strengthened using different strengthening techniques. Applying a point load at the opening joint was sufficient to cause the beam to fail in modes reported. A hydraulic jack with a capacity of 200 kN was used to apply the load at the top surface of the beam at the opening joint at a rate of 0.80 kN/sec. The ends of the beams were subjected to hinge and roller support. One Linear Variable Differential Transformer (LVDT) was attached to the bottom of the tested beams at the opening joint to measure the deflection during the loading stage. In addition, an electrical PI-shape Displacement Transducer having 50-mm gauge length was located at the vertical side of the tested beam to record the expected flexural cracks. The strain distribution in the middle reinforcing bar at the mid-length was measured using one strain gauge.

5. Test results and discussions

The observed failure modes, cracking characteristics, ultimate loading capacity, load–deflection responses, and absorbed energy capacity of the tested beams are presented herein. Table 4 presents the test results including first cracking load (P_{cr}), yield load (P_y), ultimate load (P_u), deflection recorded at P_{cr} (Δ_{cr}), cracking width measured at P_{cr} (W_{cr}), deflection recorded at P_y (Δ_y), maximum.

deflection (Δ_u), and failure modes. The P_y value was defined as the load at which the flexural steel bar reached the yield strain. Such strain was measured by strain gauges mounted on the flexural steel bar for all tested beams. The ultimate load P_u was the peaked load recorded during the test.

5.1. Cracking, yield, and ultimate loads

Generally, all tested beams had higher cracking load, yield load, and ultimate load than the control beam. From Table 4, it can be seen that P_{cr} of the tested beams is higher than that of the control beam B0. The rate of increase is 61 %, 76 %, 26 %, 38 % and 53 % for beams B1, B2, B3, B4 and B5, respectively. Similarly, P_y for beams B1, B2, B3, B4 and B5 is 47 %, 56 %, 13 %, 13 % and 22 % higher than B0, respectively. The increase in P_u of the tested beams is similar to the increase in the yield load. As can be seen from Table 4, beams B1, B2, B3, B4 and B5 had the ultimate load about 47 %, 55 %, 9 %, 24 % and 25 % higher than the B0, respectively. The experimental results show that the beam B2 had the most improvement in performance followed by beams B1, B5, B4 and

Table 5
Validation of the FE results.

Specimen ID	P_{cr}			Δ_{cr} (mm)			P_y			Δ_y (mm)			P_u			Δ_u (mm)		
	EX	FX	FE/EX	EX	FE	FE/EX	EX	FE	FE/EX	EX	FE	FE/EX	EX	FE	FE/EX	EX	FE	FE/EX
B0	66	69	1.05	3.89	3.82	0.98	97	101	1.04	8.02	7.89	0.98	110	112	1.02	28.41	26.40	0.93
B1	106	110	1.04	4.01	3.98	0.99	143	148	1.03	7.22	7.02	0.97	162	167	1.03	44.38	39.80	0.90
B2	116	121	1.04	3.56	3.45	0.97	151	156	1.03	6.05	5.88	0.97	170	177	1.04	52.57	43.10	0.82
B3	83	85	1.02	3.54	3.49	0.99	110	113	1.03	5.61	5.55	0.99	120	128	1.07	19.87	19.60	0.99
B4	91	92	1.01	3.61	3.53	0.98	110	116	1.05	5.36	5.18	0.97	136	138	1.01	45.32	42.00	0.93
B5	101	105	1.04	4.02	3.95	0.98	118	121	1.03	4.91	4.80	0.98	137	139	1.01	35.89	33.00	0.92
Avg			1.03			0.98			1.04			0.98			1.03			0.91
SD			0.01			0.01			0.01			0.01			0.02			0.05
COV			0.0024			0.00008			0.0001			0.0001			0.0005			0.003

B3, respectively when compared to the control beam B0. Therefore, the strengthening method using NSMSBs with two bars facing each other at the opening joint with $L_d = 25D_b$ is the most effective in improving the cracking, yield and ultimate loads. Then, the applications of externally bonded reinforcement (EBR) with SSPs made a satisfactory contribution to the load-carrying capacities. However, the non-rust feature of stainless-steel makes it suitable for use in corrosive environments. On the other hand, the strengthening method by attaching lower SS with anchorage bolts resulted in the least contribution to the load-carrying capacity compared to other techniques.

5.2. Cracking and failure modes

All beams were tested to failure. The cracking and failure modes of the tested beams are presented in Fig. 11. The failure modes of the tested beams are also provided in Table 4. For beam B0, the first crack was observed at the bottom surface of the beam at the opening joint at a load value about of 66 kN (about 60 % of P_u) achieving about 0.23-mm cracking width. Cracks then spread to the inclined part of the beam due to support movement. As the load was increased, the crack's width increased, and some cracks spread on the tension side. Finally, at the ultimate load, the beam failed in flexural mode as shown in Fig. 11a.

The failure of beams B1 and B2 was a typical flexural failure accompanied by pulling out of the embedded bar as shown in Fig. 11 b and c, respectively. The first cracking in the tested beams was observed at a load value about of 106 kN (about 65 % of P_u) and 116 kN (about 68 % of P_u) for beams B1 and B2, respectively. The recorded cracking width at P_{cr} was about 0.19 mm and 0.16 mm, respectively. The additional ECC layer delayed the appearance of the first crack and increased the tensile strength of the beam at the tension zone which delayed the failure of the beams. However, close to the ultimate load, major flexural cracks at the opening joint were observed as shown in Fig. 11 b and c. Furthermore, NSMSBs were pulled out which caused the surface deterioration at the bottom face. The beams B1 and B2 achieved an ultimate load of about 162 kN and 170 kN, respectively.

The failure of beam B3 was classified as a flexural failure accompanied by de-bonding of the steel sheet as shown in Fig. 11d. At a load value about of 83 kN (about 69 % of P_u) the first crack was observed at the bottom surface of the beam at the opening joint with cracking width of about 0.21 mm. As the load was increased, the width of the cracks increased, and cracks developed upward towards the loading cell. With increasing the load, the de-bonding of the steel sheet occurred at the stair joint close to the ultimate load. It was observed that the bolts pulled out as shown in Fig. 11d. It should be mentioned that the embedded length of the anchored bolts was 90 mm which was determined based on the preliminary results obtained from FE models. However, future studies should focus on the effects of the embedded length of the anchored bolts on the performance of stair beams.

For beam B4, the first crack was observed at a load of 91 kN (about 66 % of P_u) with about 0.21-mm cracking width. As can be seen in Fig. 11e, the de-bonding of SSPs on the bottom face of the beam as well as around the beam occurred as the load was close to the ultimate load. The major flexural cracks were observed at the opening joint of the beam. The beam could not resist any given load and failed at a load beyond about 136 kN. The flexural failure accompanied by separation and de-bonding of SSPs can be classified as the failure mode as shown in Fig. 11e.

For beam B5 side strengthened with SSPs, the initial crack appeared at a load value about of 101 kN (about 73 % of P_u). Flexural cracks at the opening joint initiated as the load increased and the crack's width increased as the load reached to the ultimate load. Surface de-bonding of the SSPs was observed as can be seen from Fig. 11f. The beam failure occurred at a load close to 137kN. The initial cracks became larger as the load increased and moved toward the loading cell. Major flexural cracks developed at the opening joint as the load approached the ultimate load. The flexural collapse due to de-bonding of the side SSPs can be classified

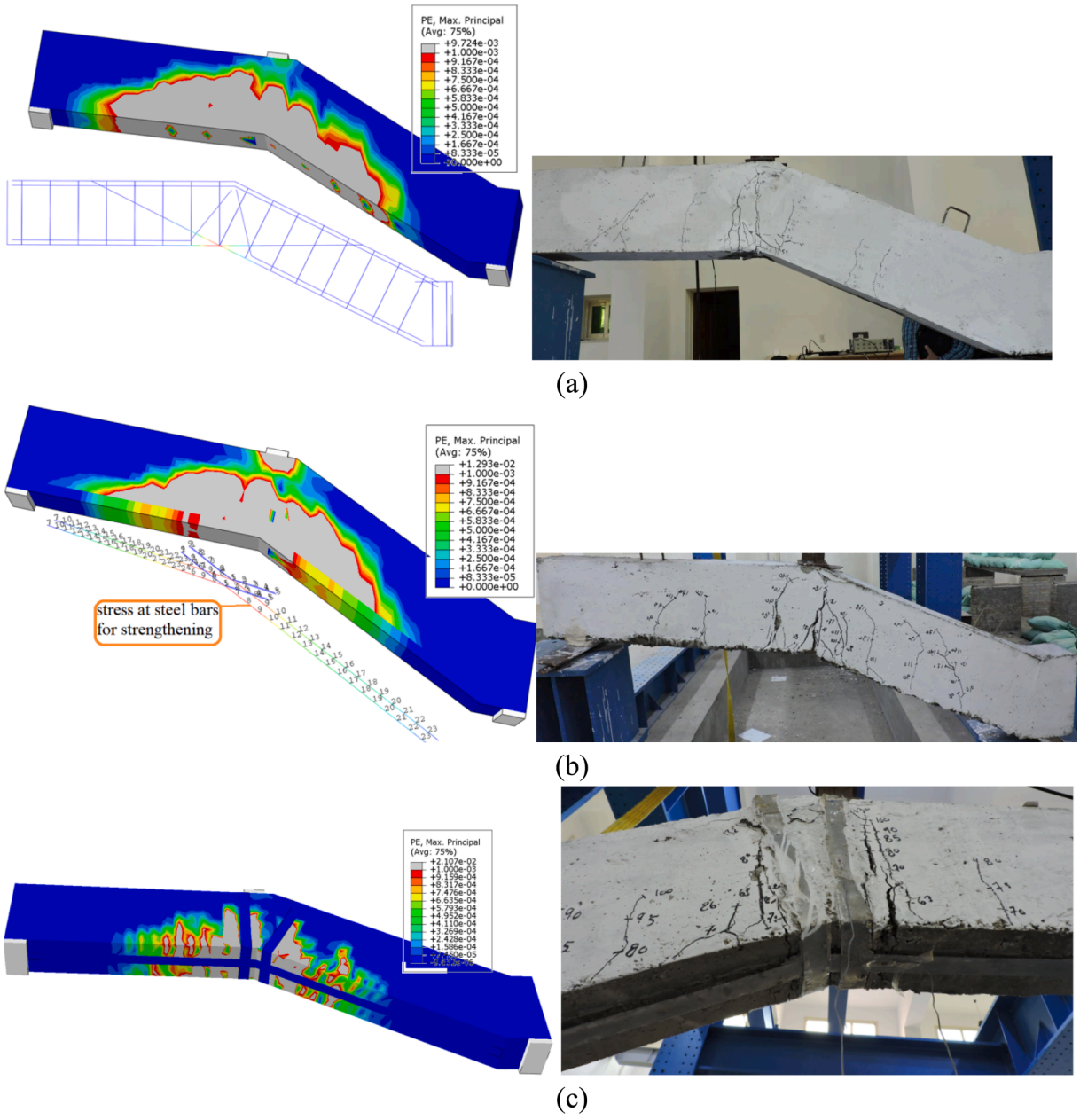

Fig. 16. Final cracks of tested beams obtained from FE analysis: (a) Master beam B0; (b) B1 and B2; (c) B4.

as the mode of failure as shown in Fig. 11f.

5.3. Load-deflection responses

Fig. 12 presents the load–deflection responses of all beams measured during the test. Table 3 also presents the mid-span deflection values corresponding to the cracking load and the maximum deflection of the tested beams. Based on the load–deflection curves, it is seen that the non-strengthened B0 behaved linearly at the un-cracked stage starting from the zero loading up to the cracking load. Then, beyond concrete cracking, B0 entered the plastic zone and experienced significant deformation, hardening up to the peaked load stage, softening performance, and then failure. All strengthened beams exhibited higher load-carrying capacities than B0. Moreover, they entered the plastic zone behaving a considerable and larger hardening with higher deflection values up to failure than the non-strengthened beam B0.

However, the differences in the pattern of the load–deflection curves depend on the method of strengthening. For beams B1 and B2, significant hardening behavior can be observed which may be attributed to the presence of ECC layer or ECC with steel bars. Then, a sudden decrease in the load values for both beams B1 and B2 was caused by the pulling-out of the embedded steel bar.

The yield deflection of beams B1, B2, B3, B4 and B5 were about 10 %, 25 %, 30 %, 33 %, and 38 %, respectively, lower than that of B0. However, for beams B1, B2, B4 and B5, the ultimate deflection was about 56 %, 85 %, 60 % and 26 %, respectively, higher than that of the control beam B0. The application of ECC improved the ultimate load of the beams and increased the ultimate deflection. In summary, the beams strengthened with either NSM with steel bars or externally bonded with SSPs had the best deflection responses compared to other beams.

5.4. Ductility index and energy absorption capacity

The absorbed energy (E) of the tested beams was determined by calculating the area under the measured load–deflection curves. Also, the ductility index computed as the ratio of ultimate deflection to the

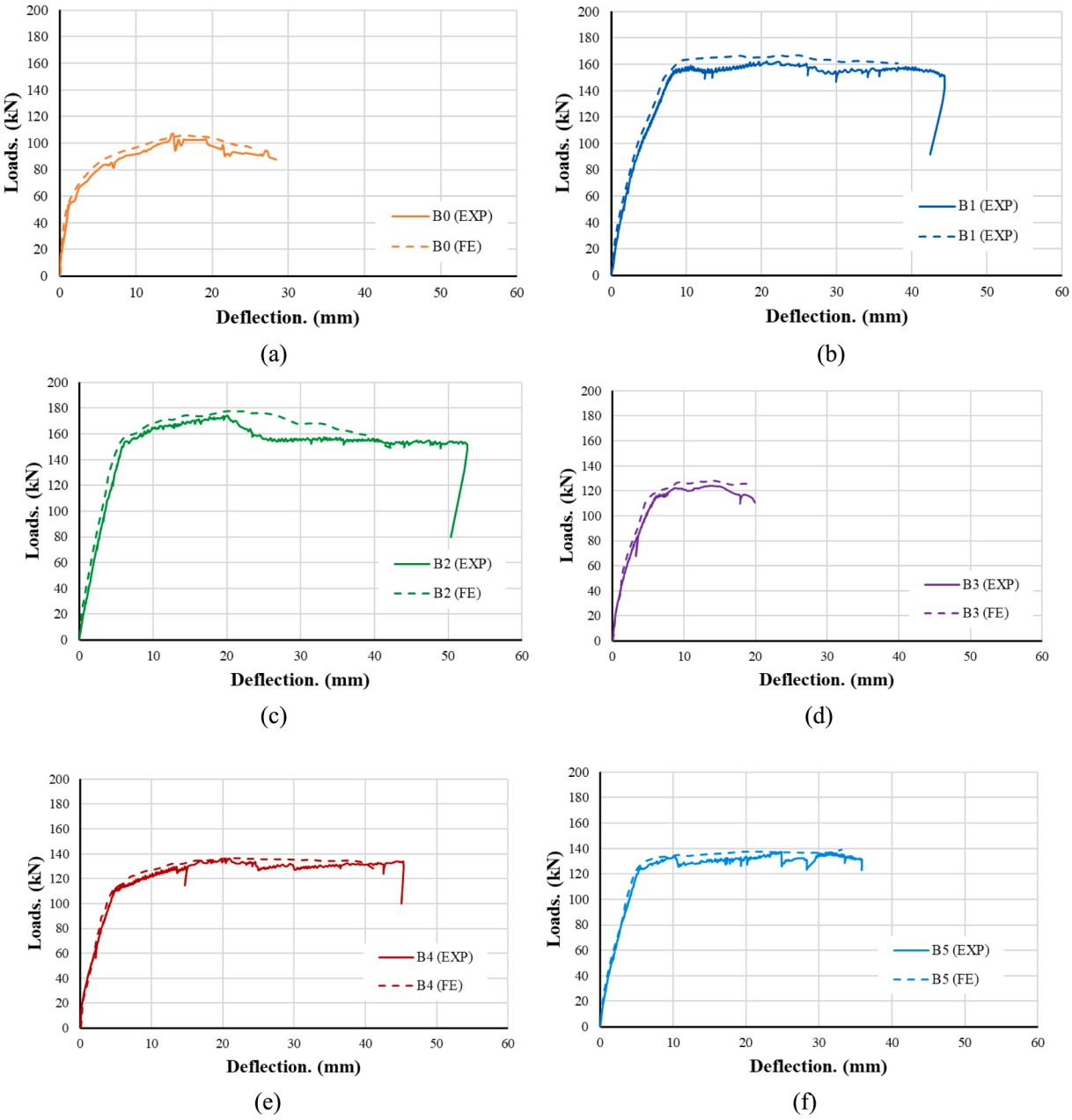

Fig. 17. Comparisons of the test and predicted load–deflection curves.

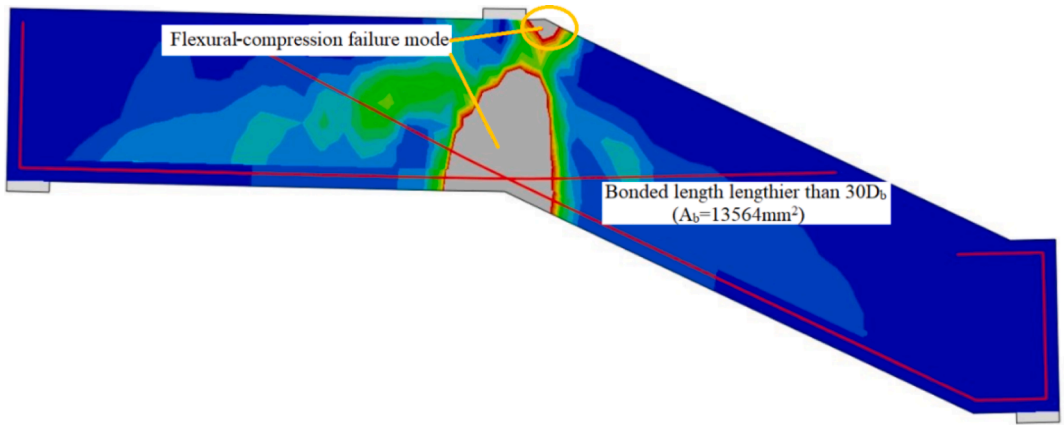

Fig. 18. Flexural-compression failure mode for FEM with L_d higher than $30D_b$ (A_b = 13564 mm^2).

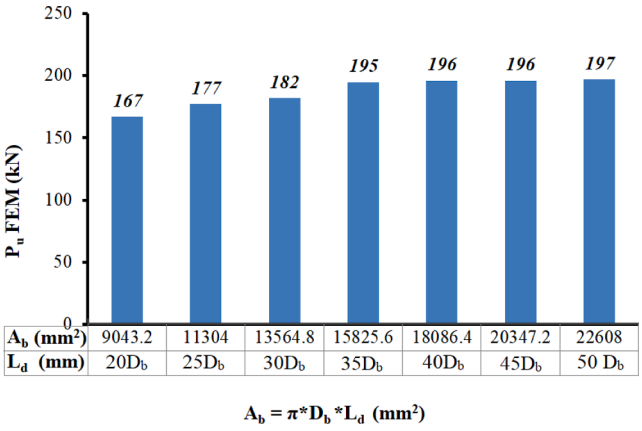

Fig. 19. Ultimate load-bar bonded area (P_u- A_b) relationship.

deflection at the yielding of the tensile reinforcement bar is presented in Table 4. The absorbed energy was used to compare the reflection of strengthening techniques and materials on the total energy consumed up to the peak load stage. It was also employed to provide further understanding of the structural efficiency of strengthened beams taking into account both elastic and plastic performance as previously reported [35]. Table 4 presents the *E* values for all tested RCSBs. Fig. 13 summarizes a schematic comparison. It is seen that *E* values for the strengthening technique of NSM with steel bars and EBR with SSPs enhanced the absorbed energy of RCSB compared to the non-strengthened one. The *E* value of RCSBs strengthened with NSMSBs was higher than that of non-strengthened ones within the range of 2.60 to 3.00 times. In this context, due to its higher strain hardening characteristics, the greater contribution to the absorbed energy was credited to the beams strengthened with the ECC layer as shown in Fig. 13. Also, The EBR with SSPs increases the E value within the range of about 1.81 to 2.21. Generally, the ductility index of all tested beams showed a significant increase compared to the control beam B0 as shown in Table 4. However, the use of steel sheet to strengthen beam B3 presented the non-satisfied enhance compared to the NC beam. This may be attributed to the shorter anchorage length used in in the opening joint.

6. Finite element modeling

The performance of tested RCSB was simulated using the Finite Element (FE) software ABAQUS [41]. The experimental results obtained in this study are used for validation purposes.

6.1. Constitutive modeling of materials and sensitivity analysis

The Concrete Damaged Plasticity (CDP) model was employed to simulate the performance of concrete. The CDP model generally predicts well the performance of concrete in RC beams; therefore, it was adopted in this study [42,43].

Several analyses have been undertaken to determine the most suitable values of the constitutive parameters used in the CDP model. The parameters related to CDP included the flow potential eccentricity (e), dilation angle (ψ), viscosity relaxation parameter (μ), the ratio of biaxial to uniaxial compressive stresses (f_{bo}/f_{co}), and the ratio of the second stress invariant on the tensile to compressive meridian (K_c). Analyses were executed with different μ values changed from 0.00 to 0.001. However, based on previous studies [9,44], it was found that $\mu = 0{,}00$ showed satisfactory numerical outcomes with lower running cost. Various trials confirmed that the angle of dilation was about 30° which was close to the value reported in previous research [44,45]. The K_c value is between 0.64 and 0.80 as previously mentioned [44]; however; the analyses conducted in this study confirmed that $k_c = 0.66$ was suitable and is a default value in ABAQUS. Also, in the present model, the default value of $e = 0.1$ in ABAQUS was selected. Several simulations have been performed with f_{bo}/f_{co} ranging from 1.10 to 1.16 based on previous reports [46,47]; however, $f_{bo}/f_{co} = 1.16$ was considered to give better results.

The measured uniaxial stress–strain responses of steel elements were idealized as a piecewise linear curve shown in Fig. 9. Fig. 8 depicts the stress–strain relationship of NC under compression and tension, which was employed in the modeling.

6.2. Model set-up, meshing and boundary conditions

Continuum, three-dimensional and eight-node linear hexahedral solid element with reduced integration (C3D8R) available in ABAQUS was employed to construct the RC beams and rigid supporting/loading steel plates as illustrated in Fig. 14. The steel rebars were represented by the two-node and linear truss element (T3D2). Four-node shell element with reduced-integration (S4R) was selected to model SS and SSPs. The mesh of the numerical model can be seen in Fig. 14. Based on the mesh sensitivity analysis, a mesh size of 12.50 mm was chosen for concrete.

It was assumed that the concrete was perfectly bonded with reinforcing bars in the RC beam to model steel bars-concrete interaction. This interaction was defined by utilizing the embedded element technique available in ABAQUS. In this technique, the RC beam was set as the host zone while the bar truss elements were defined as the embedded ones. A rigid plate of a dimension of 200 mm × 200 mm × 50 mm was used to apply load on the beams. The supports at the two ends of the beams were the same as the experimental ones where one was a roller

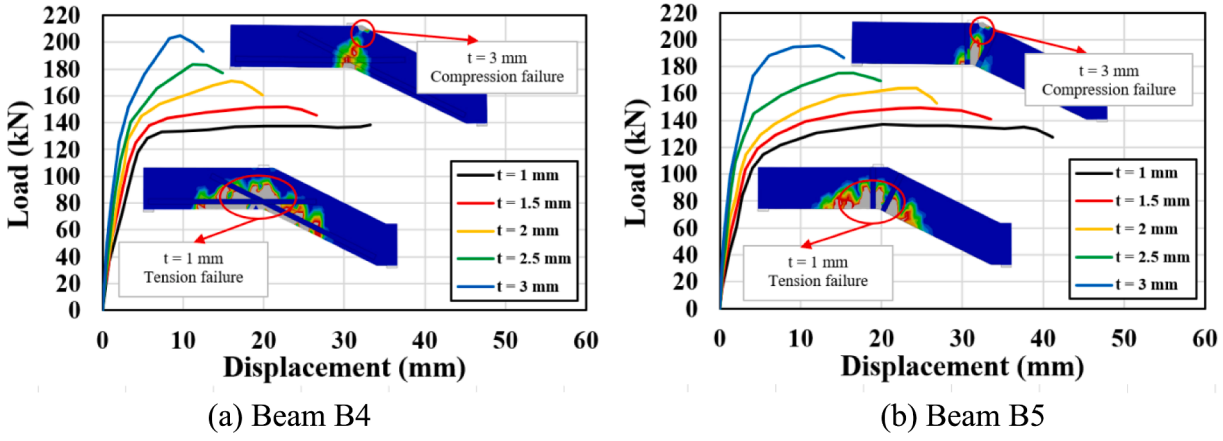

Fig. 20. Effects of plate thickness on the load–displacement responses of beams B4 and B5.

support while the other was a pinned support. Fig. 15 shows the development of the FE of the tested beams.

In order to simulate the pulling out of the steel bars at the opening bend, the interaction between the reinforcing bars and the concrete was considered with respect to Eligehausen [48]. This interaction was cohesive-damage interaction which behaves as simple bilinear traction–separation law written in terms of the effective traction τ and effective opening displacement δ. Fig. 14 shows that the relationship between the traction stress and effective opening displacement is defined by the stiffness, K_0, the local bond strength of concrete (τ_{max}), a characteristic opening displacement at fracture (δ_f), and the energy needed for opening the crack (G_{cr}) which is equal to the area under the traction–displacement curve.

The surface-to-surface tie constraint mechanism available in the ABAQUS program was delivered herein to simulate the interaction between sheets and concrete surfaces. The beam surface was the master while the steel plates were treated as slave ones. The interaction of concrete and steel sheets was modeled using the traction-separation constitutive model, which assumes the behavior as linear elastic followed by damage evolution.

7. Comparison of the test and numerical results

The accuracy of the FE model is validated by comparison of computations with the experimental data of stair beams reported in this paper. Table 5 presents the comparison of the predicted and experimental results on the cracking, yield, and ultimate stages in terms of load and deflection values. The main failure modes predicted by the FE model can be seen in Fig. 16. The load–displacement curves obtained by the FE model are compared with experimental data in Fig. 17. The FE model slightly overestimates the ultimate load of some tested beams. By comparing P_y, detected at first yield strain at flexural bars, it can be found that the enhancements are about 46 % and 54 % when using NSMSBs with 20D and 25D, respectively. For the specimens B4 and B5 where the SSPs were used, the yield load increases by about 14 % and 19 %, respectively. Also, this increase is about 23 % and 24 % for both B4 and B5, respectively. The technique applied in beam B3 led to lesser contribution to the yield load of the beam compared to the other counterparts as shown in Table 5. The mean ratios of the predicted to the measured are 1.03, 1.04 and 1.03 for the cracking, yield, and ultimate loads, respectively. The FE model generally underestimates the deflection values. The mean FE-to-EX ratio is 0.91 for the ultimate deflection, while it is about 0.98 for both the cracking and yield stages. It can be concluded that the FE model can reasonably predict the experimentally obtained performance of tested beams.

8. Parametric study

The validated FEM was employed to conduct parametric analysis on the effects of the L_d required for strengthening. Also, due to the higher capacity achieved by the planted L_d strengthening technique, both B1 and B2 were simulated by FEMs with various L_d values. To avoid the probable dispersion, the geometric parameter of L_d was selected to be the main investigated parameter while the geometry and other parameters were identical. To generalize the observed results, the area of bonded embedded length (A_b mm^2) was considered. The A_b varied from 9043.2 mm^2 to 22608 mm^2 with bonded lengths $L_d = 20D_b$ and $50D_b$, respectively. The results are discussed in terms of cracking visualization deduced numerically as shown in Fig. 18 as well as ultimate loading capacity arising from variation of embedded bar length as charted in Fig. 19. Fig. 18 illustrates that the embedded length of $30D_b$ with bar bonded area of about 13564 mm^2 can be considered the limit value to capture the ductile flexural mode. Beyond that, increasing the embedded length greater than $30D_b$ with about 13564 mm^2 results in insignificant increase in ultimate capacity. This is evidenced by the failure mode along with ultimate loads recorded by all FEMs. The failure mode of all FEMs with L_d greater than $30D_b$ is brittle flexural-compression failure mode as shown in Fig. 18.

The FE model was employed to investigate the effects of the cross-sectional area of SSPs on the performance of beams B4 and B5 by varying the thickness of SSPs from 1 mm to 1.5, 2, 2.5, and 3 mm. The width of the SSPs remained constant as 50 mm. The results obtained are provided in Fig. 20. The figure demonstrates that increasing the thickness of the SSPs improves the ultimate capacity of the strengthened beams but leads to the compression dominated failure. It is interesting to note that the beam strengthened with plate having 1-mm thickness exhibits better ductility than other beams.

9. Conclusions

This paper has presented the investigations on the effectiveness of strengthening techniques in strengthening the opening bends in RC stair beams subjected to flexural load. Experimental results on six stair beams including one un-strengthened beam taken as the control beam have been reported. The FE model was developed using ABAQUS to simulate the performance of strengthened RC stair beams. The important conclusions are summarized as follows:

(a) The application of two bottom bars with development lengths equal to twenty bar diameter (B1) and twenty-five bar diameter (B2) at the stair joint is the best method for improving the ultimate load of the beams, increasing the capacity by 47 % and 55 %, respectively.
(b) The strengthening technique using SSPs at both ends (beam B5) improved the ultimate load of the beam by 45 % and the absorbed energy by 75 % compared to the control beam.
(c) Test results show that the application of SSPs led to a moderate improvement in the ultimate load of the stair beams and better ductility than B0.
(d) The failure mode of tested beams was a flexural failure with major flexural cracks observed at the opening joint.
(e) The energy absorption capacity of all tested strengthened beams is higher than that of the control beam.
(f) The developed FEMs can reasonably simulate the experimentally measured performance of tested beams.
(g) The parametric study shows that the bonded length of $30D_b$ of the implanted embedded bar with bonded area of 13564 mm^2 was approximately the limit value for improving the ultimate load capacity of the beams. Thereafter, inconsiderable increase could be captured due to the occurrence of brittle compression failure mode.

It should be noted that the results presented in this study are valid only for this given slope of the stair beams. Nonetheless, the validated numerical model can be used to study the effects of the slope on the performance of stair beams strengthened with different techniques in the future.

CRediT authorship contribution statement

Ahmed Hamoda: Conceptualization, Methodology, Software, Validation, Formal analysis, Investigation, Data curation, Writing – original draft, Visualization, Project administration. **Mahmoud A. El-Mandouh:** Visualization, Writing – original draft. **Mizan Ahmed:** Formal analysis, Investigation, Data curation, Writing – original draft, Visualization. **Aref A. Abadel:** Visualization, Writing – review & editing, Project administration. **Qing Quan Liang:** Visualization, Writing – review & editing. **Galal Elsamak:** Formal analysis, Visualization, Writing – review & editing.

Declaration of Competing Interest

The authors declare that they have no known competing financial interests or personal relationships that could have appeared to influence the work reported in this paper.

Data availability

Data will be made available on request.

Acknowledgment

The help from technicians at Kafrelsheikh University is acknowledged. In addition, the project is supported by the Researchers Supporting Project number (RSP2023R343) provided by King Saud University, Riyadh, Saudi Arabia.

References

[1] Li B, Mosalam KM. Seismic performance of reinforced-concrete stairways during the 2008 Wenchuan earthquake. J Perform Constr Facil 2013;27(6):721–30.
[2] Bechtoula H, Ousalem H. The 21 May 2003 Zemmouri (Algeria) earthquake: damages and disaster responses. J Adv Concr Technol 2005;3(1):161–74.
[3] Afefy HM, Kassem NM, Mahmoud MH, and Taher SE-DF. Efficient strengthening of opened-joint for reinforced concrete broken slabs. Compos Struct 2016;136:602-615.
[4] Kunieda M, Denarié E, Brühwiler E, and Nakamura H, "Challenges for strain hardening cementitious composites–deformability versus matrix density," 2007.
[5] Kamal A, Kunieda M, Ueda N, Nakamura H. Evaluation of crack opening performance of a repair material with strain hardening behavior. Cem Concr Compos 2008;30(10):863–71.
[6] Kunieda M, Ueda N, Nakamura H, Tamakoshi T. Development of spraying technique for UHP-SHCC. Proc of the Concrete Structure Scenarios 2009;9:349–54.
[7] Hamoda A, Emara M, Abdelazeem F, Ahmed M. Experimental and numerical analysis of RC beams strengthened with ECC and stainless steel strips. Mag Concr Res 2022;75(5):251–70.
[8] Hamoda A, Ahmed M, Ghalla M, Liang QQ, and Abadel AA. Flexural performance of precast circular reinforced concrete members with intermediate connection filled with ultra-high-performance-concrete. Case Studies in Construction Materials 2023:e02386.
[9] Hamoda A, Ahmed M, Sennah K. Experimental and numerical investigations of the effectiveness of engineered cementitious composites and stainless steel plates in shear strengthening of reinforced concrete beams. Struct Concr 2023;24(2):2778–99.
[10] Hamoda AA, Ahmed M, Abadel AA, Ghalla M, Patel VI, Liang QQ. Experimental and numerical studies of circular precast concrete slender columns with intermediate connection filled with high-performance concrete. Structures 2023;57:105204.
[11] Li V. ECC for repair and retrofit in concrete structures. Fracture Mechanics of Concrete Structures, FRAMCOS-3 Proceedings 1998:1715-1726.
[12] Hung C-C, Chen Y-S. Innovative ECC jacketing for retrofitting shear-deficient RC members. Constr Build Mater 2016;111:408–18.
[13] Liu H, Xiao J, Ding T. Flexural performance of 3D-printed composite beams with ECC and recycled fine aggregate concrete: Experimental and numerical analysis. Eng Struct 2023;283:115865.
[14] Wu C, Li VC. CFRP-ECC hybrid for strengthening of the concrete structures. Compos Struct 2017;178:372–82.
[15] Hamoda A, Elsamak G, Emara M, Ahmed M, Liang QQ. Experimental and numerical studies of reinforced concrete beam-to-steel column composite joints subjected to torsional moment. Eng Struct 2023;275:115219.
[16] Emara M, Mohamed HA, Rizk MS, Hu JW. Behavior of ECC columns confined using steel wire mesh under axial loading. J Build Eng 2021;43:102809.
[17] Krzywoń R. Behavior of EBR FRP strengthened beams exposed to elevated temperature. Procedia Eng 2017;193:297–304.
[18] Mostofinejad D, Kashani AT. Experimental study on effect of EBR and EBROG methods on debonding of FRP sheets used for shear strengthening of RC beams. Compos B Eng 2013;45(1):1704–13.
[19] Rasheed HA, Harrison RR, Peterman RJ, Alkhrdaji T. Ductile strengthening using externally bonded and near surface mounted composite systems. Compos Struct 2010;92(10):2379–90.
[20] Nanni A, Miller B, Lorenzis L. Bond of fiber-reinforced polymer laminates to concrete. ACI Mater J 2001;98(3):256–64.
[21] Jumaat MZ, Rahman M, Rahman M. Review on bonding techniques of CFRP in strengthening concrete structures. Int J Phys Sci 2011;6(15):3567–75.
[22] Cromwell J, Harries K, Shahrooz B. Environmental durability of externally bonded FRP materials intended for repair of concrete structures. Constr Build Mater 2011;25(5):2528–39.
[23] Benzarti K, Freddi F, Frémond M. A damage model to predict the durability of bonded assemblies. Part I: Debonding behavior of FRP strengthened concrete structures. Construction and building materials 2011;25(2):547-555.
[24] Hussein M. "Strengthening of non-prismatic continuous reinforced concrete beams using CFRP," in *14th Int.* Conf. on Structural Faults and Repair: Engineering Technics Press, Edinburgh, UK; 2012.
[25] Afefy HME-D, Mahmoud MH, and Fawzy TM. Rehabilitation of defected RC stepped beams using CFRP. Engineering structures 2013;49:295-305.
[26] Ahmed M, Liang QQ, Sheikh MN, Hadi MN. Nonlinear inelastic analysis of eccentrically loaded square high-strength concrete short columns incorporating steel equal-angles. Eng Struct 2023;283:115882.
[27] Yan XF, Ahmed M, Hassanein M, He MN. Performance analysis and design of circular high-strength concrete-filled double-skin aluminum tubular short columns under axial loading. Struct Concr 2023.
[28] Ahmed M, Liang QQ, Patel VI, Hadi MN. Computational simulation of eccentrically loaded circular thin-walled concrete-filled double steel tubular slender columns. Eng Struct 2020;213:110571.
[29] Lai M, Hanzic L, Ho JC. Fillers to improve passing ability of concrete. Struct Concr 2019;20(1):185–97.
[30] Huang Z, Ho J, Cui J, Ren F, Cheng X, Lai M. Improving the post-fire behaviour of steel slag coarse aggregate concrete by adding GGBFS. Journal of Building Engineering 2023;76:107283.
[31] Lai M, Griffith A, Hanzic L, Wang Q, Ho J. Interdependence of passing ability, dilatancy and wet packing density of concrete. Constr Build Mater 2021;270:121440.
[32] Lai M, Wu K, Cheng X, Ho J, Wu J, Chen J, et al. Effect of fillers on the behaviour of heavy-weight concrete made by iron sand. Constr Build Mater 2022;332:127357.
[33] ACI 318-19. Building Code Requirements for Structural Concrete and Commentary. Farmington Hills, Michigan, USA. 2019.
[34] Rohman RK, Kristiawan SA, Saifullah HA, Basuki A. The development length of tensile reinforcement embedded in high volume fly ash-self compacting concrete (HVFA-SCC). Constr Build Mater 2022;348:128680.
[35] Hamoda AA, Eltaly BA, Sera RE, Liang QQ. Behavior of reinforced concrete stair slabs strengthened with steel plates and near surface mounted steel bars. Eng Struct 2023;292:116514.
[36] Hamoda A, Hossain K, Sennah K, Shoukry M, Mahmoud Z. Behaviour of composite high performance concrete slab on steel I-beams subjected to static hogging moment. Eng Struct 2017;140:51–65.
[37] Bolander Jr JE, Berton S. Simulation of shrinkage induced cracking in cement composite overlays. Cem Concr Compos 2004;26(7):861–71.
[38] Barros JA, Cunha VM, Ribeiro AF, Antunes J. Post-cracking behaviour of steel fibre reinforced concrete. Mater Struct 2005;38:47–56.
[39] Afefy H, Fawzy TM. Strengthening of RC one-way slabs including cut-out using different techniques. Eng Struct 2013;57:23–36.
[40] Afefy H-M-E-D, Mahmoud MH. Structural performance of RC slabs provided by pre-cast ECC strips in tension cover zone. Constr Build Mater 2014;65:103–13.
[41] Hibbitt K, Sorensen I. "ABAQUS Theory Manual, User Manual and Example Manual," ed: Simulia. RI, USA: Providence; 2000.
[42] Hamoda AA, Eltaly B, Ghalla MS. Numerical investigation on reinforced concrete closed curved beams subjected to internal pressure strengthened with sustainable material. Engineering Research Journal: ERJ; 2023.
[43] Elsamak G, Salama MI, Hamoda A. Behavior of Precast Segmental Beams Made of High-strength Concrete and Ultra-high Performance Fiber Concrete Connected by Shear Keys Technique. Arab J Sci Eng 2022:1–17.
[44] Hamoda A, Hossain K. Numerical Assessment of Slab-Column Connection Additionally Reinforced with Steel and CFRP Bars. Arab J Sci Eng 2019;44(10):8181–204.
[45] Jahani Y, Baena M, Barris C, Torres L, Sena-Cruz J. Effect of fatigue loading on flexural performance of NSM CFRP-strengthened RC beams under different service temperatures. Eng Struct 2022;273:115119.
[46] Le TT, Patel VI, Liang QQ, Huynh P, Ha NS. Numerical analysis of square concrete-filled double-skin tubular columns with outer stainless-steel tube. Struct Concr 2022;23(5):2968–85.
[47] Yu K, Wang Y, Yu J, Xu S. A strain-hardening cementitious composites with the tensile capacity up to 8%. Constr Build Mater 2017;137:410–9.
[48] Eligehausen R, Popov EP, Bertero VV. Local bond stress-slip relationships of deformed bars under generalized excitations. Earthquake Engineering Center, University of California, Berkeley, UCB/EERC-83/23; 1982.